On the Oblique Impact Dynamics of Drops on Superhydrophobic Surfaces. Part II: Restitution Coefficient and Contact Time

*Damon G. K. Aboud, Anne-Marie Kietzig**

Department of Chemical Engineering, McGill University, Montreal QC, H3A 0C5 Canada

KEYWORDS

Drops, wetting, drop impact, oblique drop impact, superhydrophobicity, Weber numbers, oblique impact, inclined surface, drop rebound, contact time, coefficient of restitution, angle of incidence.

ABSTRACT

We tested oblique drop impacts on a superhydrophobic surface at normal Weber numbers (We_n) in the range of 3 to 45, and at varying angle of incidence (AOI), ranging from 0° (normal impact) to 60° (highly oblique). Our objective is to define the influence of the angle of incidence on the restitution coefficient and on the contact time of rebounding droplets. In order to interpret the overall restitution coefficient of oblique drop rebounds (ε), we decoupled it into two separate components: a normal (ε_n) and a tangential restitution coefficient (ε_t). We discovered that,

regardless of the impact angle, ε_n can be accurately predicted as a function of the normal Weber number ($\varepsilon_n = 0.94 \cdot We_n^{-1/4}$). We support this finding with a mathematical derivation from theory, indicating a general scaling relationship of $\varepsilon_n \sim We_n^{-1/4}$ for the normal restitution coefficient. Likewise, the tangential restitution coefficient (ε_t) can also be predicted as a function of We_n ($\varepsilon_t = 1.20 \cdot We_n^{-0.12}$), but is much larger than ε_n. As a result, the overall restitution coefficient (ε) increases for more oblique impacts, since most of the tangential velocity is preserved. Furthermore, using the observed correlations for ε_n and ε_t, we derived a model to predict the overall restitution coefficient of rebounding drops at any We_n and AOI. The model's predictions are highly accurate, lying close to our experimental observations in all cases. Regarding the contact time (t_c), we found that for normal impacts, t_c increased slightly as We_n was raised. We associate this behaviour with partial penetration of the liquid into the surface's pores, which results in greater solid-liquid adhesion, prolonging detachment. For highly oblique impacts (AOI = 60°), we observed the reverse trend: the drop's contact time decreases for higher-We_n impacts. We attribute this correlation to stretched rebounding behaviour, which accelerates the rebounding of highly oblique impacts.

INTRODUCTION

Superhydrophobic (SHP) surfaces have the unique ability to cause the complete rebound of impacting water droplets. In an effort to better understand the rebounding process, researchers have been interested in characterizing specific properties, such as the restitution coefficient (ε), and the drop's contact time on the surface (t_c). And although there is already a rich body of literature pertaining to impacts occurring on flat surfaces [1-10], reports on oblique drop impacts, which are essential for the practical application of SHP surfaces, are still very rare [11-16].

Consequently, the dependence of ε and t_c with respect to the drop's angle of incidence is still entirely unknown. Accordingly, our purpose in this report is to illuminate these relationships, and to provide a new predictive power for the rebounding behaviour of drops impacting SHP surfaces under any conditions.

Generally speaking, a surface is considered superhydrophobic if it has an advancing contact angle greater than 150°, and if the contact angle hysteresis is low, usually below 10° [17]. These properties are typically observed on a surface that is chemically hydrophobic (such as a wax or PTFE), and which has a porous, air-trapping topography. This configuration allows for Cassie state wetting, in which impacting droplets interact primarily with the trapped air pockets, and make physical contact only with the topographical peaks of the surface. Consequently, drops maintain high mobility on SHP surfaces, and experience minimal adhesion [18].

The behaviour of drop impacts on SHP surfaces is typically characterized with respect to the normal Weber number, $We_n = \rho {v_{n1}}^2 D_0/\sigma$, with ρ the liquid density, v_{n1} the normal velocity of impact, D_0 the initial drop diameter, and σ the surface tension. At the moment of impact, the drop begins a spreading phase, in which the liquid's diameter increases as it deforms against the surface. For low-speed impacts ($We_n < 5$), the liquid flattens only slightly, into an ellipsoid while spreading. At higher We_n, a thin sheet of liquid (called the lamella) is expelled radially outwards from the impact center, forming a disk. In either case, as the liquid's surface tension competes with its inertia, the liquid reaches its maximum diameter, and then recedes back towards the bulk. Finally, the liquid recombines, and jumps off the surface entirely [19].

However, rebounding is not the only possible outcome. As a drop impacts a SHP surface, the liquid penetrates into the pores of the surface, driven by the force of the impact [1]. At low We_n, this causes only partial penetration, maintaining the Cassie wetting state and the mobility of the

droplet. However, at high We_n the liquid can penetrate the pores completely, expelling the air within. This prompts a transition into the Wenzel wetting state, in which the liquid makes complete contact with the solid, and adheres to the surface [1]. In this report, our discussion focuses strictly on the case of complete drop rebounding, which we observed in the range of $We_n = 3$ to 45.

From an energetic standpoint, drop rebounding is characterized by the exchange of kinetic and surface energy. As the drop deforms against the surface, some of its initial kinetic energy is converted into surface energy as the lamella extends, increasing its surface area. Meanwhile, some of the energy is consumed by viscous losses, or is transferred into modes of vibration in the rebounded droplet [2]. Because of these factors, drop rebounding is always accompanied by a net loss in energy, such that the velocity of the rebounded droplet (v_2) is less than its initial impact velocity (v_1). Hence, the restitution coefficient (ε) is defined as the ratio:

$$\varepsilon = v_2/v_1 < 1 \qquad \textbf{Equation 1}$$

Previous reports have found that the value of ε is negatively correlated with We_n [3, 6, 20, 21]. This occurs because impacts at higher We_n result in greater deformation of the droplet, so more energy is dissipated during the rebounding process, and ε decreases [6]. For water droplets impacting normally on a SHP carbon nanotube array, Aria and Gharib (2014) found that within the range of $2 < We_n < 100$, the restitution coefficient is given by $\varepsilon = 1.1 \cdot {We_n}^{-1/4}$ [3].

Another essential characterization of drop rebounding is the contact time (t_c). This parameter is especially important in the design of anti-icing SHP surfaces, since a shorter t_c allows for less heat transfer between the surface and drop, which inhibits freezing [22]. Richard et al. (2002) performed drop rebounding experiments in a range of We_n = 0.3 to 37, and found that the contact time can be predicted by the following equation [4]:

$$t_c = \beta \sqrt{\frac{\rho {D_0}^3}{8\sigma}} = \beta \cdot \tau_{ic} \qquad \textbf{Equation 2}$$

The term $\sqrt{\rho {D_0}^3/\sigma}$ is the inertial-capillary timescale (τ_{ic}), which is related to the lowest vibrational period of a freely oscillating drop [5]. The contact time factor (β) is experimentally determined, and relates the actual contact time to τ_{ic}. Richard's original measurements indicate that $\beta = 2.6$, a value which has been corroborated by other researchers [4, 6].

Interestingly, **Equation 2** implies that the contact time is independent of the impact speed, and instead depends solely on the properties of the droplet. In general, this relationship holds true [4, 6], but there are a number of factors that can influence the value of β, thereby altering t_c. For example, Bird et al. (2013) tested rebounding behaviour on a SHP surface with a large ridge that split drops in half upon impact. Since the resulting halves of the drop were smaller than the original, the contact time factor was reduced to only $\beta = 1.6$ [5]. Liu et al (2014) reported a new behavior called pancake bouncing, in which the drop rebounds before the retraction phase, with a factor as low as $\beta = 0.53$ [23]. This behaviour is possible on surfaces with precisely tuned microstructures, such that the liquid penetrating the surface's pores is ejected by capillary forces near the end of the spreading phase. Moreover, in a previous report we introduced the stretched rebound behaviour, where an oblique impacting droplet detaches from the surface while still outstretched, with β as low as 1.32 [11]. Similar to pancake bouncing, this behaviour is caused by the capillary ejection of the liquid from the pores of the SHP surface, but occurs only in oblique impacts [12].

Oblique drop impacts are more complex than the normal case because the drop's angle of incidence against the surface can change the interaction entirely. This allows for new behaviours such as sliding, one-sided splashing, and stretched rebounding [11]. **Figure 1** demonstrates the

orientation of our oblique drop impact experiment, and illustrates the variables involved. In **Figure 1(a)**, we see a water droplet falling downwards with a velocity of v_d, onto the surface with a tilt angle of θ, which is moving horizontally at a surface velocity of v_s. **Figure 1(b)** presents the same system, but taking the surface as the point of reference. In this orientation, the drop's impact velocity with respect to the surface is v_1, and can be further broken down into two components: the normal velocity ($v_{n1} = v_s\, sin(\theta) + v_d\, cos(\theta)$), and the tangential velocity ($v_{t1} = v_s\, cos(\theta) - v_d\, sin(\theta)$). Accordingly, the angle of incidence of the impact is given by:

$$AOI = tan^{-1}(v_{t1}/v_{n1}) \qquad \textbf{Equation 3}$$

Thus, normal impacts occur at AOI = 0°, and oblique impacts occur at higher AOI. It is also important to note that the angle of incidence is different than the surface tilt angle (θ). The angle of incidence takes the surface as the point of reference, thus accounting for the surface velocity. Consequently, the surface tilt and the AOI are only equal for a surface at rest.

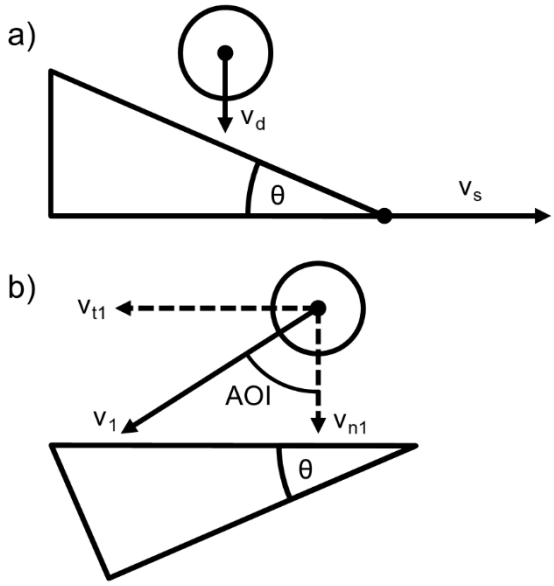

Figure 1. Schematic of our oblique drop impact experiment. (a) a drop falls downwards with a velocity of v_d, onto a surface moving at a velocity of v_s, with a surface tilt of θ. (b) The same drop

and surface as above, but taking the surface as the frame of reference. The drop's impact velocity (v_1) can be separated into a tangential (v_{t1}) and a normal (v_{n1}) component. The angle of incidence of the impact depends on v_{n1} and v_{t1}.

Presently, there are very few oblique drop impact studies that address either the contact time or the restitution coefficient of rebounding drops [12-16]. And, of the few studies in place, all were performed using a stationary surface, which has led to a common limitation. In a laboratory setting, the falling velocity of drops (v_d) is restrained by aerodynamic drag (usually to below about 2 m/s). And, since the normal Weber number is further reduced by the tilt angle of the surface (θ), stationary surface experiments are subject to a trade-off: experiments can be performed either at low θ to maintain a good range of We_n, or at a high surface tilt, but with low We_n. For example, Zhu et al. (2017) measured the change in t_c as θ was raised, but worked only in the region of $\theta = 0$ - 30° [15]. Other publications have elected to perform all of their experiments at a single surface tilt angle [12, 13, 16], or else to hold v_d constant while changing θ [14].

While all of the publications listed above have proven insightful, their experimental methods compound We_n and the AOI, and hence cannot explain how these parameters affect the impact behaviour individually. As a result, it is not currently possible to predict the rebounding behaviour over a wide range of conditions. To address this problem, we have developed an experimental setup that accelerates our sample surface to high velocities, allowing us to test any We_n and AOI desired. This has allowed us to create a novel experimental space: while holding We_n constant, the angle of incidence is raised, and the changes in the contact time and the restitution coefficient are measured. And, since neither of these variables has been measured before using these methods, our analysis is entirely novel. Also, note that this report is the second in a two-part publication

series; in part I, we addressed the sliding length and maximum spread diameter of oblique impacts using the same methods.

EXPERIMENTAL

To synthesize our superhydrophobic surface, we began with a 0.8 mm thick polished PTFE sheet, with one bondable side (McMaster Carr). Femtosecond laser micromachining was applied to fabricate a surface structure. The focused laser beam was raster scanned across a 0.8×3 cm patch to ablate the material, developing a hierarchical topography: a wavy microstructure, composed of a wiry nanostructure (**Figure 2(c)**). This procedure is outlined more comprehensibly in our previous publication [11].

The wetting properties of our sample surface were characterized via goniometry. First, the sample was cleaned ultrasonically in an acetone bath. Once dry, the dynamic advancing and receding contact angles of a deionized water droplet were measured using a Data Physics OCA 15E goniometer. The drop was placed on the surface with an initial volume of 4 μL. Then, the volume was raised up to 7 μL, at a pace of 0.1 μL/s. The drop was then allowed to rest for 5 seconds, after which the volume was reduced to 1 μL, at 0.1 μL/s. Three measurements were preformed, with an average advancing contact angle of $157.6 \pm 2°$, receding contact angle of $156.2 \pm 2°$, and a contact angle hysteresis is $1.4 \pm 0.7°$ ($\pm$ 2 st. dev.).

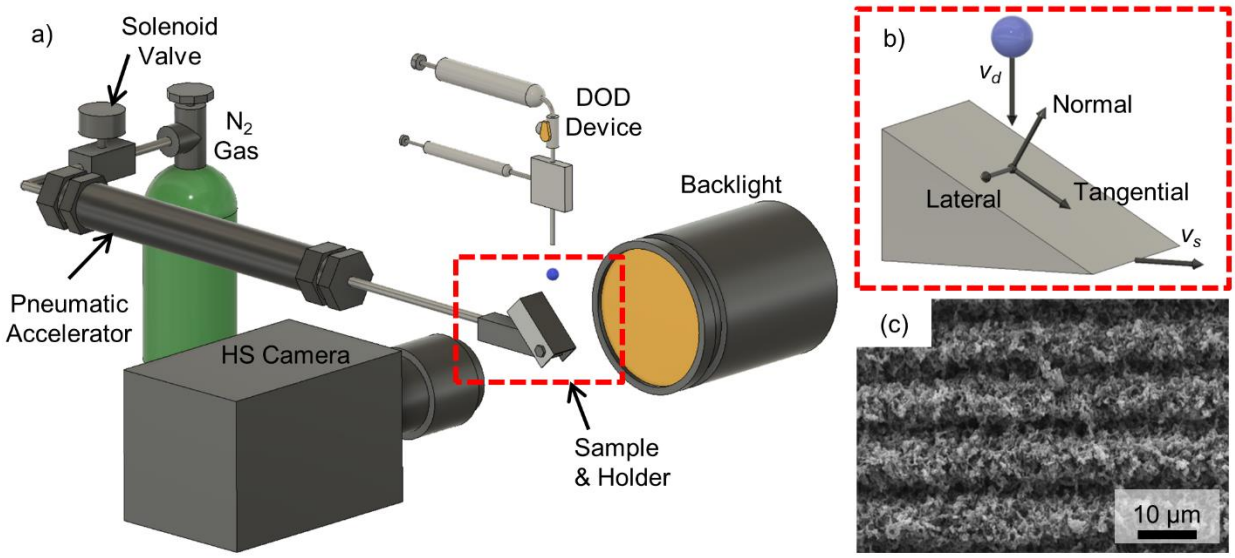

Figure 2. (a) 3D schematic of the drop impact apparatus. (b) Visualization of the orientation of the experiment. The camera is aligned so that the normal and tangential dimensions are visible, but the lateral direction is not observed. (c) Scanning electron microscope image of the sample SHP surface.

Our experimental setup is illustrated in **Figure 2(a)**. The sample SHP surface is attached to an aluminum sample holder using epoxy (H.L. Plasto, 1402). The sample's orientation is such that the crests and troughs of the microstructure run along the lateral direction, as indicated in **Figure 2(b)**. The sample holder allows for surface tilt angles in the range of 0 - 90°, and is driven forward by a pneumatic accelerator. A drop-on-demand (DOD) generator provides monodisperse droplets that fall downward onto the sample as it moves. For full details on this device, see Wood el al. (2018) [24]. Synchronization between the pneumatic accelerator and the DOD was accomplished using an Arduino Mega 2560 microcontroller prototyping board (Arduino Company). Impact events were recorded by a Photron SA5 high-speed camera, fitted with a Navitar Macro Zoom

7000 lens. Backlighting was provided by an AI SL185-WHI-IC Ultra Bright Spot Light (Optikon Corp.).

Measurement of the restitution coefficient was performed using MATLAB codes. Using a series of high-speed video snapshots, the drop's center of mass was tracked over the course of the its impact and rebound trajectories. This data was used to calculate v_1 at the moment of impact, and v_2 at the moment of detachment.

The average drop diameter of our experiments was 1.30 ± 0.07 mm (±2 st. dev.). Throughout this report, time is presented in dimensionless form with respect to the inertial-capillary timescale ($t^* = t/\tau_{ic}$). All values presented for the restitution coefficient and contact time in this report are the average of 4 measurements. All error bars and margins of error represent two standard deviations of the data. In this report, our analysis focuses strictly on the case of complete rebounding drops, with no fragmentation. Therefore, we tested We_n in the range of 3 to 45, above which we began to observe partial rebound. The average values of We_n and the AOI in our experiments are outlined in **Table 1**. Note that for brevity, our discussion section will refer to the nearest integer values of We_n. And for aesthetic purposes, we will refer to the average angles of incidence as 0°, 30°, 45° and 60°, instead of their precise decimal values. The exact conditions of an impact are stated where relevant.

Table 1. Data set average values of the normal Weber number and angle of incidence among experiments.

We_n
3.0 ± 0.4
8.8 ± 1.3
23.7 ± 1.6
44.6 ± 3.5
AOI
0.2° ± 0.9
29.5° ± 2.1
45.6° ± 2.5
60.8° ± 1.7

RESULTS & DISCUSSION

RESTITUTION COEFFICIENT

The restitution coefficient (ε) provides information about the transfers between kinetic and surface energy during the rebounding process. In our experiment, we observed complete rebounding of impacting droplets in the range of $We_n = 3$ to 45. **Figure 3** plots ε versus We_n, for each angle of incidence tested. In each case, we observe that as We_n is increased, ε decreases, indicating that impacts at high speed lose more energy in the rebounding process. Furthermore, as the AOI increases, ε also increases. This indicates that impacts at higher AOI rebound with a higher velocity, and therefore retain more of their initial kinetic energy.

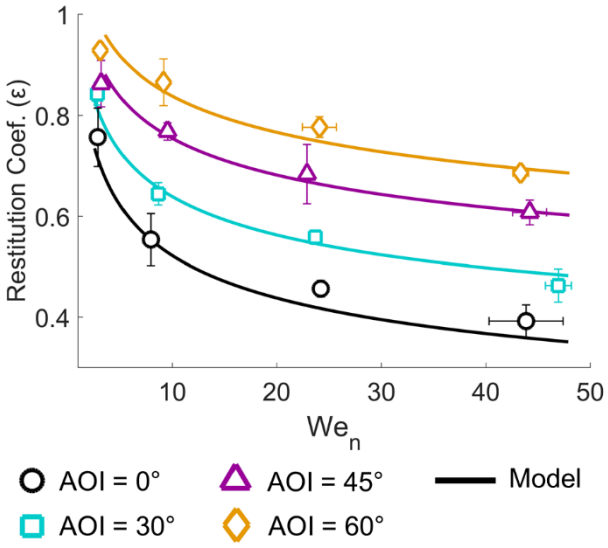

Figure 3. Plot of the restitution coefficient versus the normal Weber number for rebounding drops. The solid lines represent our model (**Equation 14**).

To explain these observations, we must first define two separate components of ε. The normal restitution coefficient is equal to $\varepsilon_n = v_{n2}/v_{n1}$, where v_{n2} is the normal velocity of the drop as it detaches from the surface. Similarly, the tangential restitution coefficient ($\varepsilon_t = v_{t2}/v_{t1}$) relates the drop's impacting and rebounding (v_{t2}) tangential velocities. **Figure 4** plots ε_n and ε_t versus We_n at different AOI. Our analysis will focus first on the normal restitution coefficient.

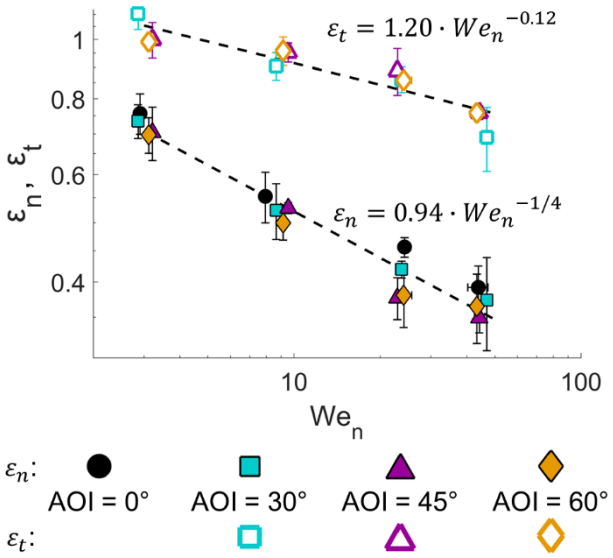

Figure 4. The normal restitution coefficient (ε_n) and the tangential restitution coefficient (ε_t) versus the normal Weber number.

From **Figure 4**, we see that ε_n (filled markers) ranges from about 0.75 to 0.35, dropping monotonically as We_n increases. And interestingly, ε_n remains relatively constant with respect to the angle of incidence, such that the value over the course of our entire experimental range can be approximated by a first-order regression ($R^2 = 0.95$):

$$\varepsilon_n = 0.94 \cdot We_n^{-1/4} \qquad \textbf{Equation 4}$$

Equation 4 is consistent with the results of Aria and Gharib (2014), who also measured the rebounding of water drops on a flat SHP surface. They found that in the range of $We_n = 2$ to 100, the restitution coefficient of their SHP surface could be described by the correlation $\varepsilon_n = 1.1 \cdot We_n^{-1/4}$. They also collected data from several different sources and found that the restitution coefficient follows the general scaling law $\varepsilon_n = a \cdot We_n^{-1/4}$ [3], where the factor a varies among different SHP surfaces depending on their exact properties. For example, comparing Aria's

measurement of $a = 1.1$ to our measurement of 0.94, we see that their surface reflected drops with a slightly higher restitution coefficient than our laser machined PTFE surface did.

Although the scaling relationship of $\varepsilon_n = a \cdot {We_n}^{-1/4}$ has been previously reported [3], it has not yet been explained. Thus, we offer the following derivation from theory, by considering the transfer of kinetic and surface energy during the rebounding process. As a drop impacts a SHP surface, its kinetic energy is transferred into surface energy as the lamella spreads outwards into a disk. For the case of lossless energy transfer, one would expect that the lamella's maximum spread area (A_{max}) should scale as $A_{max} \sim We_n$ [7]. However, due to viscous dissipation, the true relationship is approximately $A_{max} \sim {We_n}^{1/2}$ [7-10]. Therefore, since $We_n \sim {v_{n1}}^2$, it follows that:

$$A_{max} \sim v_{n1} \qquad \textbf{Equation 5}$$

Next, we include a key contribution from Gilet and Bush (2012), who used image processing to directly measure both the kinetic and surface energy at each stage throughout the process of drop impact and rebound. Their experimental results confirm a proportionality first proposed by Biance et al. (2006): during the lamella's retraction phase, the kinetic energy returned to the rebounding droplet (KE_2) is directly proportional to the maximum stored surface energy while outstretched (SE_{max}), so that $KE_2 \sim SE_{max}$ [6, 25]. In that case, since $KE_2 \sim {v_{n2}}^2$, and the drop's maximum spread area is proportional to the stored surface energy ($A_{max} \sim SE_{max}$), it follows that v_{n2} is correlated with A_{max} by the relationship:

$${v_{n2}}^2 \sim A_{max} \qquad \textbf{Equation 6}$$

Figure 5 tests this assertion empirically, plotting v_{n2}^2 versus A_{max} for normal impacts. Indeed, a linear regression fits the data well ($R^2 = 0.96$), confirming **Equation 6**. Combining **Equation 5**

and **Equation 6**, we find an interesting relationship between the velocities of the drop before and after impact:

$$v_{n2} \sim \sqrt{v_{n1}} \qquad \textbf{Equation 7}$$

And, substituting this relationship back into the original formula for the restitution coefficient ($\varepsilon_n = v_2/v_1$), we can relate ε_n directly to v_{n1}:

$$\varepsilon_n \sim \frac{\sqrt{v_{n1}}}{v_{n1}} \sim {v_{n1}}^{-1/2} \qquad \textbf{Equation 8}$$

Finally, considering that $v_{n1} \sim {We_n}^{1/2}$, we conclude that:

$$\varepsilon_n \sim {We_n}^{-1/4} \qquad \textbf{Equation 9}$$

which matches our results exactly. Thus, by considering viscous energy losses during the spreading phase, as well as the transfer of surface energy into kinetic energy during retraction, we can explain the observed relationship of $\varepsilon_n \sim {We_n}^{-1/4}$. And, although this scaling relationship has been previously reported through empirical analysis [3], we contribute here the mathematical derivation to support the aforementioned experimental results.

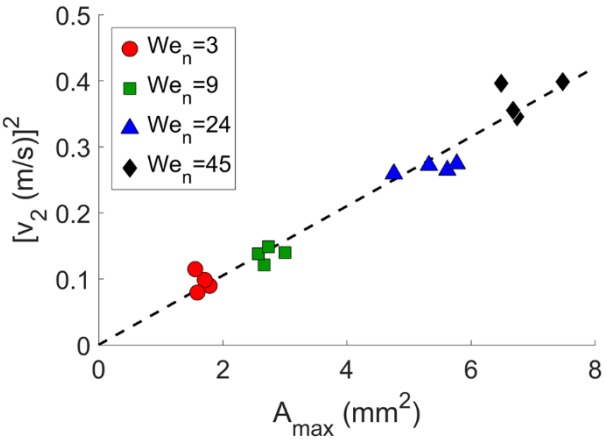

Figure 5. For impacts at normal angle of incidence, the square of the velocity of the rebounded drop is proportional to its maximum spread area on the surface.

For comparison, it should be noted that our findings contrast with those of Biance et al. (2006), who measured ε_n of Leidenfrost drop bouncing on a heated Silicon surface, and found that ε_n scales as $\varepsilon_n \sim We_n^{-1/2}$, instead of $\varepsilon_n \sim We_n^{-1/4}$. This discrepancy is surprising, considering that the two processes are extremely similar. Moreover, Biance presented a theoretical derivation of their equation based on a mass-and-spring model, that is also generalizable to the case of drop rebound on SHP surfaces. Nevertheless, since **Equation 9** agrees with Aria et al. (2014) [3], and is supported by the theoretical derivation presented above, we suggest that the normal restitution coefficient of drop rebounding on SHP surfaces scales as $\varepsilon_n \sim We_n^{-1/4}$, and that Biance's equation pertains specifically to the case of Leidenfrost bouncing of drops.

Looking back at **Figure 4**, the tangential restitution coefficient also drops monotonically as We_n increases, and shows no obvious correlation with the AOI. Accordingly, ε_t can be modeled by a linear regression ($R^2 = 0.86$), indicated by the dashed line in **Figure 4**:

$$\varepsilon_t = 1.20 \cdot We_n^{-0.12} \qquad \textbf{Equation 10}$$

It is also evident in **Figure 4** that that ε_t is much larger than ε_n in our experiment. Therefore, where the drop loses much of its normal velocity after rebound, its tangential velocity is hardly affected by the interaction, such that v_{t2} is very close to v_{t1}. For example, at $We_n = 24$, ε_n is equal to about 0.4, while ε_t close to 0.9. As illustrated in **Figure 6**, the discrepancy between the values of ε_n and ε_t leads to an interesting feature of oblique impacts: the drop's angle of rebound ($AOR = tan^{-1}(v_{t2}/v_{n2})$) is greater than its angle of incidence. In the figure, the drop impacts at AOI = 45°, and rebounds with AOR = 67°, indicating a shift of 22° in the angle. This occurs because the drop's normal velocity is reduced much more during impact than the tangential velocity, which

leads to a shift in the ratio of v_t/v_n, and therefore a change in the drop's trajectory with respect to the surface.

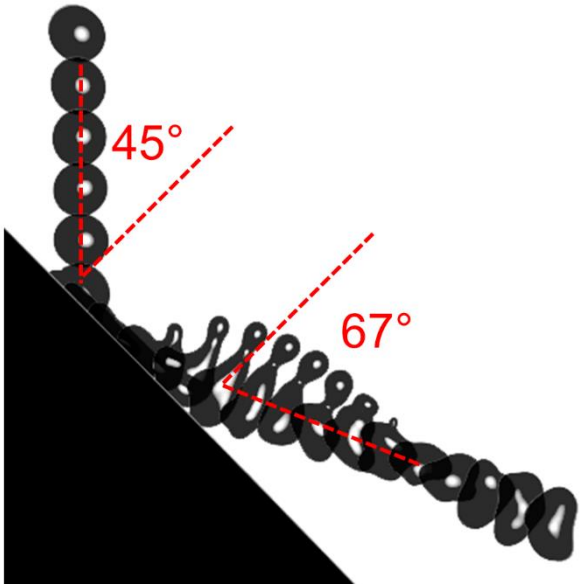

Figure 6. Composite image of a drop rebounding ($We_n = 22.6$, AOI = 45.2°). The angle of incidence (AOI) and the angle of rebound (AOR) are both indicated by dashed red lines. The AOR is always higher than the AOI on our surface.

The values of the normal and tangential restitution coefficients are so different because the mechanisms that govern ε_t are entirely different than those governing ε_n. As discussed above, ε_n depends on the transfers between kinetic and surface energy as the drop deforms and rebounds off of the SHP surface. In contrast, we suggest that ε_t is determined by the adhesion properties of the surface. As a drop impacts a SHP surface, the liquid penetrates into the pores of the surface, establishing sites of solid-liquid contact. And, since higher-We_n impacts penetrate deeper into the pores of the surface [1], the drop may experience greater adhesion, and lose more speed. We attribute the negative correlation between ε_t and We_n to this mechanism.

Now, having characterized both ε_n and ε_t, we present a model for the overall restitution coefficient (ε) of an oblique impact. We begin with the velocity of the reflected drop, which is a function of its normal and tangential components:

$$v_2 = \sqrt{{v_{n2}}^2 + {v_{t2}}^2} \qquad \textbf{Equation 11}$$

And by definition, $\varepsilon_n = v_{n2}/v_{n1}$ and $\varepsilon_t = v_{t2}/v_{t1}$:

$$v_2 = \sqrt{(\varepsilon_n v_{n1})^2 + (\varepsilon_t v_{t1})^2} \qquad \textbf{Equation 12}$$

Now, the normal and tangential impact velocities can be stated in terms of the drop's impact velocity (v_1) and the AOI, so that $v_n = v_1 \cos(AOI)$ and $v_t = v_1 \sin(AOI)$. Substituting these two expressions, along with the definition of the restitution coefficient ($\varepsilon = v_2/v_1$) into **Equation 12**, we find a general expression for the restitution coefficient as a function of its components:

$$\varepsilon = \sqrt{(\cos(AOI) \cdot \varepsilon_n)^2 + (\sin(AOI) \cdot \varepsilon_t)^2} \qquad \textbf{Equation 13}$$

Finally, substituting **Equation 4** and **Equation 10** for ε_n and ε_t, we arrive at the following expression, predicting the restitution coefficient of oblique drop impacts at any We_n and AOI:

$$\varepsilon \simeq \sqrt{(0.94 \cos(AOI) \cdot {We_n}^{-1/4})^2 + (1.20 \sin(AOI) \cdot {We_n}^{-0.12})^2} \qquad \textbf{Equation 14}$$

Figure 7 plots **Equation 14** along with the original data. The model provides a good description of the experimental data, with all points lying very close to the lines. In addition, **Supporting Note 1** presents a logarithmic plot of ε versus We_n, along with some continued discussion for the interested reader.

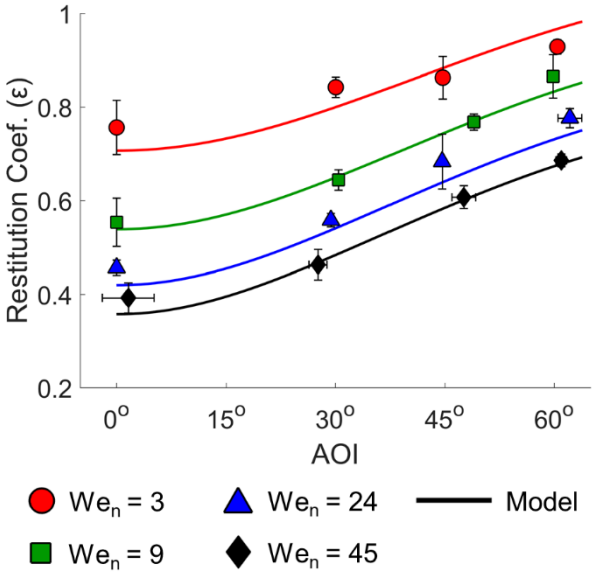

Figure 7. Restitution coefficient versus the angle of incidence for each We_n tested. The solid lines represent our model (**Equation 14**).

Regarding the application of our model, it is important to note that **Equation 14** must be adjusted somewhat to suit the exact surface in question. This is because **Equation 14** is derived using empirical relationships for ε_n and ε_t, both of which vary among different superhydrophobic surfaces. For example, we have demonstrated that while the normal restitution coefficient follows the general scaling law $\varepsilon_n = a \cdot We_n^{-1/4}$, the factor a changes slightly among different SHP surfaces. Furthermore, we expect that ε_t will also vary among different surfaces, depending on their adhesion properties. Therefore, the relationship between both ε_n and ε_t versus We_n must be determined empirically for any SHP surface before substituting them into **Equation 14**. Nevertheless, although factors within the equation may vary slightly, our method of derivation is applicable to any superhydrophobic surface, and can be used to accurately predict the restitution coefficient of drops rebounding on a SHP surface at any We_n and AOI.

Furthermore, **Equation 14** might also be adaptable for the case of Leidenfrost drop bouncing. As previously discussed, Biance et al. (2006) demonstrated that the normal restitution coefficient of Leidenfrost drop bouncing scales as $\varepsilon_n = a \cdot We_n^{-1/2}$ [6], which could be substituted into the first term of **Equation 14** (in place of **Equation 4**). And, although we are not aware of any published correlation between ε_t and We_n for Leidenfrost drops, it is reasonable to assume that the relationship also follows the general form $\varepsilon_t = b \cdot We_n^{-c}$. Therefore, we predict that the oblique rebounding process, as well as the overall restitution coefficient of Leidenfrost droplets, is very similar to that of drops on SHP surfaces, except with small changes to the scaling relationships with We_n.

CONTACT TIME

The contact time (t_c) of a droplet is the period during which it remains in contact with the surface, from the first moment of impact until detachment. Quantitatively, the contact time is best understood by considering the value of the contact time factor (β) from **Equation 2**, which relates t_c to the drop's inertial-capillary timescale ($t_c = \beta \cdot \tau_{ic}$). **Figure 8(a)** plots β versus the AOI for each We_n tested, and **Figure 8(c)** provides high-speed video snapshots for visual reference. At each We_n and AOI tested in this report, we observe complete rebounding of the drops, with no secondary droplets remaining on the surface. Considering first the contact time at normal angle of incidence (AOI = 0°), we observe that β increases monotonically with each increase in We_n. Sectioned in the red box in **Figure 8(c)**, the snapshots clearly demonstrate how the contact time increases for higher-We_n impacts at normal angle of incidence. This positive correlation has been previously observed, and our results are consistent with those of Deng et al. (2013) [8].

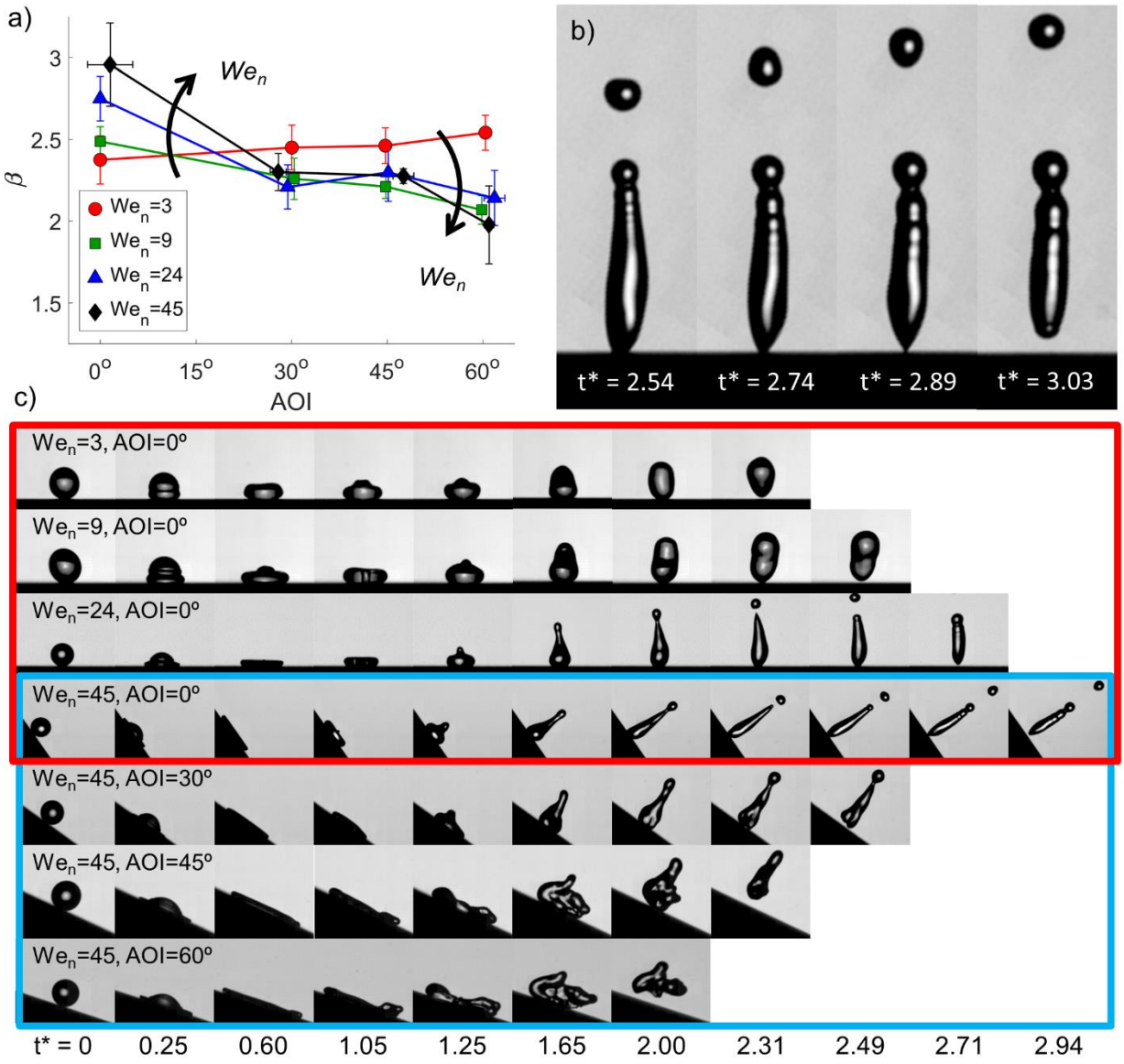

Figure 8. (a) The contact time factor (β) and We_n are positively correlated at AOI = 0°, but negatively correlated at AOI = 60°. (b) Expanded and rotated view of a drop impact at $We_n = 44.6$, AOI = 2.2° (full set of snapshots shown in (c)), highlighting the drop's process of detachment from the surface. (c) High-speed video snapshots of selected drop impacts. Note that since both β and the dimensionless time (t^*) are calculated with respect to τ_{ic}, at the moment of detachment t^* is equal to β. Also, note that since all experiments at $We_n = 45$ (blue box) were performed on moving surfaces, the AOI differs from the surface tilt angle (θ). The values of We_n and AOI stated

in the figure are for the data set average. The exact parameters of the selected videos are (from top to bottom): $We_n = 3.2$ & AOI = 0.0°, $We_n = 8.0$ & AOI = 0.0°, $We_n = 23.7$ & AOI = 0.0°, $We_n = 44.6$ & AOI = 2.2°, $We_n = 47.3$ & AOI = 27.5°, $We_n = 47.5$ & AOI = 48.3°, $We_n = 53.2$ & AOI = 58.6°.

However, **Equation 2** indicates that the contact time is dependent only on the properties of the droplet, and not on the impact velocity. Therefore, at first glance, our results appear to contradict theory. But this difference can be readily explained. Impacts at higher We_n cause more partial penetration of the liquid into the microstructure of the SHP surface [1]. This increases the adhesion, such that after the lamella's retraction phase, as the drop begins to move away from the surface, some of the liquid remains adhered to the surface. This is demonstrated in **Figure 8(b)**, which provides enlarged snapshots of an impact at $We_n = 44.6$, AOI = 2.2°, focusing on the moments before and after detachment. Looking at the first three frames, we see that before detachment, the drop's center of gravity has already moved well away from the surface, and contact is being maintained only by a small point at the base of the drop. Although the liquid at that point has not made the full transition into the Wenzel wetting regime, it is still deeply entrenched in the complex structure of the surface, and requires work to remove. Moments later ($t^* = 3.03$), the drop's surface tension finally overcomes the solid-liquid adhesion at the interface, and pulls the liquid away from the surface entirely. The reason that higher-We_n impacts take longer to achieve full detachment is because the liquid penetrates more deeply into the pores of the surface, and requires more force to remove.

Beyond the normal impact case, some interesting trends emerge in the behaviour of oblique drop rebounds. Looking qualitatively at the snapshots in **Figure 8(c)**, the observed contact angles at the

front and the tail of the drops are unequal in many of the images. This results from the drop's tangential movement across the surface during the rebound process. During most of the impact, the lamella's front is advancing quickly across the surface, and therefore meets the surface at approximately the advancing contact angle. At the other end, the lamella's tail is receding as the drop slides across the surface, and thus has a contact angle close to the receding contact angle. This effect is especially visible in the lowest row of snapshots in **Figure 8(c)** at $t^* \leq 1.05$. In these images, the left side of the drop (the front edge) has a noticeably higher contact angle than the tail.

Regarding the contact time of oblique impacts, for $We_n = 3$ we observe a mild increase in β as AOI increases, changing from 2.36 to 2.53 as AOI increases from 0° to 60°, respectively. Conversely, for all of the higher We_n impacts measured, β decreases over the same range of angles. The most significant change occurs at $We_n = 45$, for which β drops from 2.99 to 1.94. **Figure 8(c)** illustrates this difference visually with high-speed video snapshots of drops rebounding at $We_n = 45$, for AOI ranging from 0° to 60°. Sectioned in the blue box in the figure, these images clearly demonstrate the reduction of β as the angle of incidence increases. This likely owes to the presence of stretched rebounding behaviour. Much like the pancake bouncing behaviour reported by Liu et al. (2014) [23], stretched rebounding occurs when the capillary ejection of the penetrating liquid in the microstructure provides vertical lift to the lamella [12]. In **Figure 8(c)**, this effect is most obvious for the impact at $We_n = 45$ and AOI = 60° between $t^* = 1.05$ and 1.65, in which the tail of the lamella begins lifting from the surface. This initiates a peeling effect from the lamella's tail towards the center, accelerating the detachment of the liquid from the SHP surface.

Moreover, looking at **Figure 8(a)** and comparing the data for AOI = 0° and 60°, the hastening effect of stretched rebounding results in another interesting observation: where the value of β was

positively correlated with We_n for normal impacts, the trend reverses for highly oblique impacts, such that β is negatively correlated with We_n at AOI = 60°. As a result, for these highly oblique impacts, β drops from 2.5 to 1.94 as We_n is increased from 3 to 45.

It is interesting to note that partial penetration of the impacting liquid into the microstructure is responsible for both the positive correlation between β and We_n at AOI = 0°, as well as the negative correlation at AOI = 60°. Although t_c has been previously measured on either a normal [8] or tilted surfaces [12], we are the first to measure t_c versus the AOI, so the overall trends have not yet been reported. However, these trends are not universal, and would change for a SHP surface with a different topography. For example, Antonini et al. (2014) performed normal drop impacts with varying We_n, and found no correlation between We_n and β [14]. Regarding oblique impacts, we associate our observed drop in β as AOI increases with stretched rebounding. However, Zhang et al. (2017) demonstrated that the stretched rebounding behaviour is not present on every SHP surface, and varies significantly with changes in the topography [12]. Both of these comparisons lend towards the same point: it is not currently possible to predict the relationship between β, We_n, and AOI without manually testing the surface. Therefore, as a topic of future research, we recommend that the contact time of oblique drop impacts should be measured on many SHP surfaces with different topology, in order to clarify the governing factors.

CONCLUSIONS

We have designed a novel drop impact experiment in which a tilted surface can be accelerated to high velocities, allowing us to observe and measure highly oblique drop impacts. Using this

apparatus, we observed rebounding drops on a superhydrophobic surface at normal Weber numbers (We_n) in the range of 3 to 45, and at varying angle of incidence (AOI), ranging from 0° (normal impact) to 60° (highly oblique). This experimental space has allowed us to characterize the influence of the AOI on the dynamics of oblique drop impacts. This report is part II of a two-part publication series, and focuses on the restitution coefficient (ε) and on the contact time (t_c) of rebounding drops. In part I, our analysis covered the sliding length and the maximum spreading diameter of drops during impact. Hence, our contribution allows for the accurate prediction of the impact behaviour of drops under any impact conditions.

Concerning the restitution coefficient, we decoupled ε into two separate components: the normal (ε_n) and the tangential restitution coefficients (ε_t). We discovered that, regardless of the drop's angle of incidence on the surface, ε_n can be accurately calculated as a function of the normal Weber number ($\varepsilon_n = 0.94 \cdot We_n{}^{-1/4}$). To explain this relationship, we considered the transfers between kinetic and surface energy as the drop deforms against the SHP surface and rebounds. By accounting for the viscous dissipation of energy during this process, we derived from theory the general relationship of $\varepsilon_n \sim We_n{}^{-1/4}$, which is consistent with our observations, as well as with the empirical conclusions of other reports.

As for the tangential component, we found that ε_t can also be predicted as a function of We_n ($\varepsilon_t = 1.20 \cdot We_n{}^{-0.12}$). In addition, we found that ε_t is much larger than ε_n, such that very little of the drop's tangential velocity is lost during the rebound process. This is because, where ε_n is governed by viscous dissipation, ε_t is governed by an entirely separate mechanism: solid-liquid adhesion occurring between the drop and the SHP surface. Because ε_t is much larger than ε_n, the overall restitution coefficient (ε) increases for higher-AOI (more oblique) impacts, since more of the drop's overall momentum is preserved. Furthermore, using the equations stated above for ε_n

and ε_t, we derived a model to predict ε for any We_n and AOI. The model's predictions are highly accurate, lying close to our experimental observations across our entire experimental space.

Regarding the drop's contact time on the surface at normal AOI, t_c increased slightly for higher-We_n impacts. We associate this behaviour with the partial penetration of the liquid into the pores of the surface, which increases the area of solid-liquid contact between the drop and surface, resulting in greater adhesion. For highly oblique impacts (AOI = 60°), we observed the reverse trend: the drop's contact time decreases for higher-We_n impacts. We attribute this correlation to stretched rebounding behaviour, which can occur in highly oblique impacts, and helps the drop to detach from the surface more quickly [12].

ASSOCIATED CONTENT

Supporting Information. Continued discussion on the scaling relationship between ε and We_n (Supporting Note 1).

AUTHOR INFORMATION

Corresponding Author

*Anne-Marie Kietzig, McGill University, Department of Chemical Engineering 3610 University Street, Montreal, Quebec, H3A 0C5, Canada, email: anne.kietzig@mcgill.ca.

Author Contributions

Damon Aboud designed and performed the experiments, and wrote the manuscript. Prof. Anne-Marie Kietzig guided the project and edited the manuscript. All authors have given approval to the final version of the manuscript.

Funding Sources

This work was supported by the Natural Sciences and Engineering Research Council (NSERC) of Canada.

ACKNOWLEDGMENT

The authors acknowledge Dr. Daniel Gagnon of the Institut de Recherche d'Hydro-Québec (IREQ) for the financial support.

REFERENCES

1. Maitra, T.; Tiwari, M. K.; Antonini, C.; Schoch, P.; Jung, S.; Eberle, P.; Poulikakos, D. On the Nanoengineering of Superhydrophobic and Impalement Resistant Surface Textures Below the Freezing Temperature. *Nano Lett.* **2013**, 14, 172-182.

2. Richard, D.; Quéré, D. Bouncing Water Drops. *Europhys. Lett.* **2000**, 50, 769.

3. Aria, A. I.; Gharib, M. Physicochemical Characteristics and Droplet Impact Dynamics of Superhydrophobic Carbon Nanotube Arrays. *Langmuir* **2014**, 30, 6780-6790.

4. Richard, D.; Clanet, C.; Quéré, D. Contact Time of a Bouncing Drop. *Nature* **2002**, 417, 811.

5. Bird, J. C.; Dhiman, R.; Kwon, H.-M.; Varanasi, K. K. Reducing the Contact Time of a Bouncing Drop. *Nature* **2013**, 503, 385-388.

6. Biance, A.-L.; Chevy, F.; Clanet, C.; Lagubeau, G.; Quéré, D. On the Elasticity of an Inertial Liquid Shock. *J. Fluid Mech.* **2006**, 554, 47-66.

7. Clanet, C.; Béguin, C.; Richard, D.; Quéré, D. Maximal Deformation of an Impacting Drop. *J. Fluid Mech.* **2004**, 517, 199-208.

8. Deng, X.; Schellenberger, F.; Papadopoulos, P.; Vollmer, D.; Butt, H.-J. r. Liquid Drops Impacting Superamphiphobic Coatings. *Langmuir* **2013**, 29, 7847-7856.

9. Tsai, P.; Hendrix, M. H.; Dijkstra, R. R.; Shui, L.; Lohse, D. Microscopic Structure Influencing Macroscopic Splash at High Weber Number. *Soft Matter* **2011**, 7, 11325-11333.

10. Meng, K.; Jiang, Y.; Jiang, Z.; Lian, J.; Jiang, Q. Impact Dynamics of Water Droplets on Cu Films with Three-Level Hierarchical Structures. *J. Mater. Sci.* **2014**, 49, 3379-3390.

11. Aboud, D. G.; Kietzig, A.-M. Splashing Threshold of Oblique Droplet Impacts on Surfaces of Various Wettability. *Langmuir* **2015**, 31, 10100-10111.

12. Zhang, R.; Hao, P.; He, F. Drop Impact on Oblique Superhydrophobic Surfaces with Two-Tier Roughness. *Langmuir* **2017**.

13. Ramachandran, R.; Sobolev, K.; Nosonovsky, M. Dynamics of Droplet Impact on Hydrophobic/Icephobic Concrete with Potential for Superhydrophobicity. *Langmuir* **2015**.

14. Antonini, C.; Villa, F.; Marengo, M. Oblique Impacts of Water Drops onto Hydrophobic and Superhydrophobic Surfaces: Outcomes, Timing, and Rebound Maps. *Exp. Fluids* **2014**, 55, 1-9.

15. Zhu, J.; Deng, D. Ammonia-Assisted Wet-Chemical Synthesis of Zno Microrod Arrays on Substrates for Microdroplet Transfer. *Langmuir* **2017**.

16. Yeong, Y. H.; Burton, J.; Loth, E.; Bayer, I. S. Drop Impact and Rebound Dynamics on an Inclined Superhydrophobic Surface. *Langmuir* **2014**, 30, 12027-12038.

17. Li, X.-M.; Reinhoudt, D.; Crego-Calama, M. What Do We Need for a Superhydrophobic Surface? A Review on the Recent Progress in the Preparation of Superhydrophobic Surfaces. *Chem. Soc. Rev.* **2007**, 36, 1350-1368.

18. Barthlott, W.; Neinhuis, C. Purity of the Sacred Lotus, or Escape from Contamination in Biological Surfaces. *Planta* **1997**, 202, 1-8.

19. Rioboo, R.; Tropea, C.; Marengo, M. Outcomes from a Drop Impact on Solid Surfaces. *Atomization Sprays* **2001**, 11, 155-165.

20. Chen, L.; Xiao, Z.; Chan, P. C.; Lee, Y.-K.; Li, Z. A Comparative Study of Droplet Impact Dynamics on a Dual-Scaled Superhydrophobic Surface and Lotus Leaf. *Appl. Surf. Sci.* **2011**, 257, 8857-8863.

21. Bertola, V. An Experimental Study of Bouncing Leidenfrost Drops: Comparison between Newtonian and Viscoelastic Liquids. *Int. J. Heat Mass Transfer* **2009**, 52, 1786-1793.

22. Mishchenko, L.; Hatton, B.; Bahadur, V.; Taylor, J. A.; Krupenkin, T.; Aizenberg, J. Design of Ice-Free Nanostructured Surfaces Based on Repulsion of Impacting Water Droplets. *Acs Nano* **2010**, 4, 7699-7707.

23. Liu, Y.; Moevius, L.; Xu, X.; Qian, T.; Yeomans, J. M.; Wang, Z. Pancake Bouncing on Superhydrophobic Surfaces. *Nat. Phys.* **2014**.

24. Wood, M. J.; Aristizabal, F.; Coady, M.; Nielson, K.; Ragogna, P. J.; Kietzig, A.-M. The Precise and Accurate Production of Millimetric Water Droplets Using a Superhydrophobic Generating Apparatus. *Phys. Fluids* **2018**, 30, 027104.

25. Gilet, T.; Bush, J. W. Droplets Bouncing on a Wet, Inclined Surface. *Phys. Fluids* **2012**, 24, 122103.

SYNOPSIS

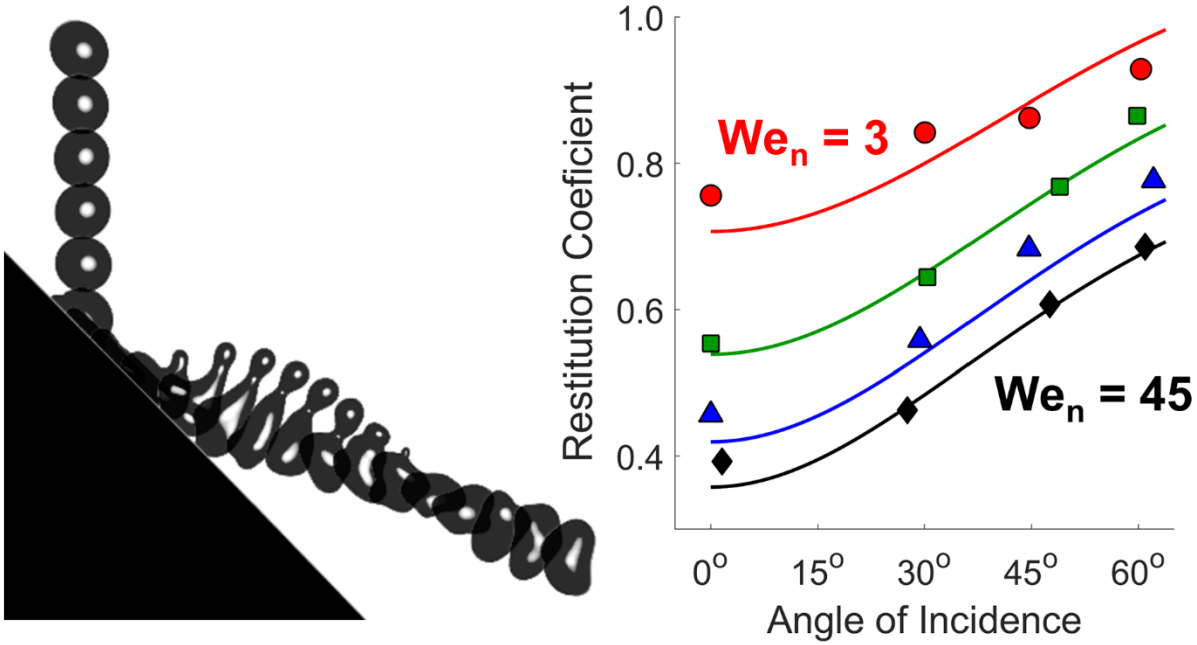

The left side of the TOC graphic shows a compound image of a drop undergoing complete rebound on our SHP surface. The right side shows our experimental data for the restitution coefficient of rebounding drops at different normal Weber numbers and angles of incidence, along with our derived model.

SUPPORTING NOTE 1: CONTINUED DISCUSSION ON THE SCALING RELATIONSHIP BETWEEN ε AND We_n

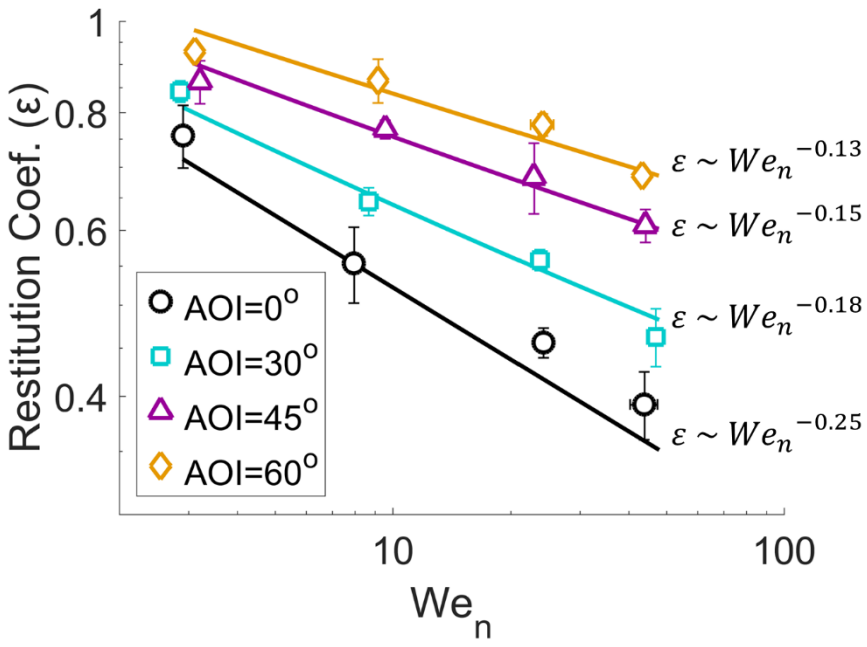

Figure S1. Restitution coefficient versus the normal Weber number for each AOI tested, on logarithmic axes. The correlations to the right describe the average slope of the model's lines, which are almost perfectly linear in this format.

As a point of interest, **Figure S1** presents the same data as **Figure 3** in the main text, but on logarithmic axes. In this format, **Equation 14** is almost perfectly linear, and included in the figure are the average slopes of each model line, which determine the correlation between ε and We_n at each angle tested. For AOI = 0°, we find that $\varepsilon_t \sim We_n^{-0.25}$, which matches **Equation 4**. However, as the AOI is raised, the correlation gradually shifts towards $\varepsilon_t \sim We_n^{-0.13}$ at AOI = 60°, which is very close to **Equation 10** ($\varepsilon_t = 1.20 \cdot We_n^{-0.12}$). This shift serves as a perfect demonstration, explaining why the restitution coefficient is higher for more oblique impacts. At low AOI, ε is approximately equal to ε_n, whose value is relatively low. However, as the AOI rises, the value of

ε approaches the value of ε_t, which is much higher. This allows more oblique impacts to rebound with a greater restitution coefficient.